Vol. 15, No. 4, 2024
ISSN 2233-4203/ e-ISSN 2093-8950
ARTICLE www.msletters.org | Mass Spectrometry Letters

Metabolism of Magnolin in Human and Rat Hepatocytes Using Liquid Chromatography-High Resolution Mass Spectrometry

Min Seo Lee, Eun Jeong Kim, and Hye Suk Lee*

Drug Metabolism & Bioanalysis Laboratory, College of Pharmacy, The Catholic University of Korea, Bucheon 14662, Korea

Received December 6, 2024, Revised December 16, 2024, Accepted December 17, 2024
First published on the web December 31, 2024; DOI: 10.5478/MSL.2024.15.4.202

Abstract : Magnolin, a bioactive lignan separated from Flos Magnoliae, possesses anti-inflammatory, anticancer, antioxidant, and vasodilator effects. This study compared the metabolic profiles of magnolin in human and rat hepatocytes using liquid chromatography-high resolution mass spectrometry. The hepatic extraction ratio of magnolin in human and rat hepatocytes were 0.27 and 0.14, respectively, suggesting that it undergoes a low-to-moderate degree of hepatic metabolism. During metabolism in human hepatocytes, magnolin generated 8 phase 1 metabolites, including *O*-desmethylmagnolin (M1-M4), hydroxymagnolin (M5), di-*O*-desmethylmagnolin (M6 and M7), and hydroxy-*O*-desmethylmagnolin (M8), and 11 phase 2 metabolites, including glucuronides of M1-M4 (M9-M12) and M7 (M15), sulfates of M1, M2, M6, and M7 (M13, M14, and M16-M18), and M6 disulfate (M19). However, 6 phase 1 metabolites (M1-M5 and M8) and 6 phase 2 metabolites (M9-M14) were formed after incubation of magnolin with rat hepatocytes. These findings help to predict the pharmacokinetics and metabolism of magnolin in humans.

Keywords : magnolin; hepatocytes; in vitro metabolism; LC-HRMS

Introduction

Magnolin, a major component of Flos Magnoliae, has demonstrated multiple pharmacological activities, including anti-inflammatory, anticancer, antioxidant, and vasodilator effects.[1-3] Magnolin can suppress cell migration and invasion in lung cancer by targeting the ERKs/RSK2 signaling pathway and also exhibits tumor cell growth by inducing cell cycle arrest via the p53/P21 pathway.[4, 5] Additionally, magnolin inhibits colorectal cancer growth by inducing autophagy and cell cycle arrest via the LIF/Stat3/Mcl-1 pathway.[6]

During the development of a new drug, drug candidates are selected based on efficacy and pharmacokinetic attributes, such as clearance, oral bioavailability, and metabolic profile. During the preclinical development stage, it is necessary to characterize *in vitro* metabolism of drug candidate in human and animal hepatocytes, the gold standard model for *in vitro* metabolism studies.[7-9] There are a few studies on the pharmacokinetics and metabolism of magnolin in rats.[10,11] Based on intravenous and oral pharmacokinetics of magnolin in the rats, magnolin was rapidly absorbed (bioavailability, 54.3-76.4%) and was almost eliminated by nonrenal route such as the metabolism.[10] After oral administration of magnolin in rats, magnolin was metabolized to 4′-*O*-desmethylmagnolin, 4″-*O*-desmethylmagnolin, and their respective glucuronides.[11] Human liver microsomal incubation of magnolin with reduced nicotinamide adenine dinucleotide phosphate (NADPH) at 37°C resulted in the formation of *O*-desmethylmagnolin, di-O-desmethylmagnolin, and hydroxymagnolin via CYP2C8, CYP2C19, CYP2C9, and CYP3A4 enzymes.[12] Magnolin did not inhibit CYP1A2, CYP2A6, CYP2B6, CYP2C8, CYP2C9, CYP2C19, CYP2D6, CYP3A4, UGT1A4, UGT1A6, UGT1A9, and UGT2B7 enzyme activities in human liver microsomes but weakly inhibited UGT1A1- and UGT1A3-mediated glucuronidation with K_i values of 26.0 μM and 37.6 μM, respectively.[13,14] However, there was no report on the metabolism of magnolin in human and animal hepatocytes.

In the present study, phase 1 and phase 2 metabolic pathways of magnolin in human and rat hepatocytes were characterized using liquid chromatography-high resolution mass spectrometry (LC-HRMS) to evaluate the species difference in magnolin metabolism and predict the drug exposure levels and safety of magnolin in humans.

*Reprint requests to Hye Suk Lee
https://orcid.org/0000-0003-1055-9628
E-mail: sianalee@catholic.ac.kr

Materials and Methods

Materials and Reagents

Magnolin (purity, 99.98%), medioresinol (purity, 98.88%), and kobusin (purity, 99.93%; internal standard) were obtained from MedChemExpress (Monmouth Junction, NJ, USA). NADPH, 3-phosphoadenosine-5-phosphosulfate (PAPS), β-glucuronidase from *Escherichia coli*, sulfatase from *Helix pomatia*, and uridine 5'-diphosphoglucuronic acid (UDPGA) were obtained from Sigma-Aldrich Co. (St. Louis, MO, USA). Pooled human liver microsomes, pooled human liver S9 fraction, and pooled rat liver microsomes were obtained from Corning Life Sciences (Woburn, MA, USA). Cryopreserved human and rat hepatocytes, optiincubate hepatocyte media, and OptiThaw cryohepatocyte kit were purchased from XenoTech (Kansas City, KS, USA). Acetonitrile, methanol, and water (HPLC grade) were obtained from Thermo Fischer Scientific (Fair Lawn, NJ, USA). All other chemicals were of the highest quality available.

Metabolic stability of magnolin in human and rat hepatocytes

To evaluate the metabolic stability of magnolin in human and rat hepatocytes, pooled cryopreserved hepatocytes were carefully thawed in recovery medium and resuspended in Krebs–Henseleit buffer to achieve a final density of 5×10^5 cells/mL. Then, 60 μL hepatocyte suspension and an equal volume of 1 μM magnolin in the incubation medium were mixed in 96-well plates and incubated in triplicate for 0, 10, 20, 30, 45, 60, 90, and 120 min at 37°C in a CO_2 incubator. Next, 120 μL ice-cold kobusin (internal standard, 500 ng/mL) in acetonitrile was added to each well and the mixtures were sonicated for 5 min, followed by centrifugation at 13,000 rpm for 10 min at 4°C. An aliquot of each supernatant was transferred to an autosampler vial, and 5 μL supernatant was analyzed via LC-HRMS.

Metabolite profiling of magnolin in hepatocytes and liver preparations

To identify *in vitro* metabolites of magnolin, 60 μL aliquots of human or rat hepatocyte suspensions (5×10^5 cells/mL) and an equal volume of 10 μM magnolin in the incubation medium were mixed in 96-well plates and incubated for 2 h in a CO_2 incubator at 37°C. 120 μL ice-cold acetonitrile was added to each well and the mixtures were sonicated for 5 min, followed by centrifugation at 13,000 rpm for 10 min at 4°C. The supernatants were evaporated to dryness using a vacuum concentrator. The residues were dissolved in 100 μL 30% methanol and 5 μL aliquots were injected into the LC-HRMS system.

To identify the glucuronidation of phase 1 metabolites, M1-M4, and M7, 100 μL reaction mixture containing 50 mM potassium phosphate buffer (pH 7.4), 10 mM magnesium chloride, human liver microsomes (20 μg protein), 1 mM NADPH, 5 mM UDPGA, and 10 μM magnolin or medioresinol was incubated at 37°C for 30 min. The reactions were quenched by adding 100 μL acetonitrile. After centrifugation, the supernatants were evaporated to dryness using a vacuum concentrator. The residues were dissolved in 100 μL 30% methanol and 5 μL aliquots were injected into the LC-HRMS system.

For the enzymatic hydrolysis of glucuronide metabolites, 20 μL aliquot of magnolin-treated human hepatocyte incubates was incubated with 20 μL of β-glucuronidase (4000 units/mL) in 50 mM potassium phosphate buffer (pH 6.8) for 2 h at 37°C. The reactions were quenched by adding 40 μL acetonitrile. After centrifugation, the supernatants were evaporated to dryness using a vacuum concentrator. The residue was dissolved in 35 μL of 30% methanol.

For the enzymatic hydrolysis of sulfate metabolites, 20 μL aliquot of magnolin-treated human hepatocyte incubates was incubated with 20 μL of sulfatase (1000 units/mL) in 200 mM sodium acetate buffer (pH 5.0) for 2 h at 37°C. The reactions were quenched by adding 40 μL acetonitrile. After centrifugation, the supernatants were evaporated to dryness and the residue was dissolved in 35 μL of 30% methanol.

LC-HRMS analysis

To identify magnolin and its metabolites, we used a Q-Exactive Orbitrap mass spectrometer (Thermo Fisher Scientific) coupled with Nexera X2 UPLC (Shimadzu, Kyoto, Japan). Magnolin and its metabolites were separated on a Halo C18 column (2.1 × 100 mm, 2.7 μm; Advanced Material Technology, Wilmington, DE, USA) via gradient elution using 5% methanol in 10 mM ammonium formate (mobile phase A) and 95% methanol (mobile phase B) at a flow rate of 0.30 mL/min: 30% mobile phase B for 0.5 min, 30% to 38% mobile phase B over 9.5 min, 38% to 45% mobile phase B over 2 min, 45% mobile phase B for 6 min, 45% to 60% mobile phase B over 7 min, 60% to 90% mobile phase B over 0.1 min, 90% mobile phase B for 2.9 min, 90% to 30% mobile phase B over 0.1 min, and 30% mobile phase B for 3.9 min. The column and autosampler temperatures were 40°C and 4°C, respectively. Accurate mass values of magnolin and its metabolites were measured via positive electrospray ionization, with the following electrospray source settings: capillary temperature, 350°C; aux gas heater temperature, 300°C; spray voltage, 3.5 kV; nitrogen sheath gas, 40 arbitrary units; auxiliary gas, 10 arbitrary units; and collision dissociation energy, 10 eV. Full scan MS1 with the data-dependent MS2 acquisition mode was used to obtain MS scan data ranging from *m/z* 100 to 1000 with resolution of 70,000. Data were processed using Xcalibur software version 2.2 (Thermo Fisher Scientific). The product ion structures were analyzed using Mass Frontier software (version 6.0; HighChem Ltd., Bratislava, Slovakia).

Results and Discussion

The metabolic parameters such as elimination half-life, intrinsic clearance, hepatic clearance, and hepatic extraction ratio of magnolin in human and rat hepatocytes were calculated using their physiological parameters such as liver weight and hepatic blood flow[7-9,15] (Table 1). The hepatic extraction ratios of magnolin obtained from incubations of human and rat hepatocytes were 0.27 and 0.14, respectively, indicating that magnolin was moderately metabolized in human hepatocytes but low metabolized in rat hepatocytes according to the decision criteria described by Bohnert and Gan[15], suggesting the low-to-moderate hepatic metabolism of magnolin. The hepatic clearance value (7.8 mL/min/kg) in rat hepatocytes was comparable to the systemic clearance value (14.3-17.6 mL/min/kg) following intravenous injection of magnolin in male SD rats[10], suggesting that hepatic metabolism is the major clearance pathway of magnolin in rats and humans. Therefore, we further characterized the metabolite profiling of magnolin in human and rat hepatocytes.

Incubation of magnolin with human and rat hepatocytes resulted in the formation of 19 and 12 metabolites, respectively. The extracted ion chromatograms of magnolin, 8 phase 1 metabolites (M1-M8), and 11 phase 2 metabolites (M9-M19) are shown in Figure 1. The retention time, elemental composition, observed molecular ion, mass error, and biotransformation of magnolin and its 19 metabolites are summarized in Table 2.

Magnolin showed $[M+H]^+$ ion at *m/z* 417.19031 as a molecular ion in MS spectrum and the characteristic product ions at *m/z* 399.18030 (loss of water from $[M+H]^+$ ion), *m/z* 328.13077 (Figure 2A, fragment g), *m/z* 279.12270 [4-(3,4,5-trimethoxyphenyl)tetrahydro-1*H*,3*H*-furo[3,4-

Table 1. Metabolic stability parameters of magnolin after incubation of 1 μM magnolin with human and rat hepatocytes at 37°C

Parameters	Human hepatocytes	Rat hepatocytes
Half-life (min)	154.4	168.1
intrinsic clearance (mL/min/kg)	32.1	38.6
hepatic clearance (mL/min/kg)	5.5	7.8
hepatic extraction ratio	0.27	0.14

Table 2. Retention time (t_R), elemental composition, and molecular ion ($[M+H]^+$ or $[M+NH_4]^+$) of magnolin and its possible metabolites after 2 h incubation with human and rat hepatocytes

Metabolites	t_R (min)	Elemental composition	*m/z* ($[M+H]^+$, $[M+NH_4]^+$)*	Mass error (ppm)	Biotransformation	Hepatocytes	
						Human	Rat
Magnolin	20.74	$C_{23}H_{28}O_7$	417.19031	-1.13	-	-	-
M1	13.94	$C_{22}H_{26}O_7$	403.17496	-0.42	*O*-demethylation	○	○
M2	14.87	$C_{22}H_{26}O_7$	403.17487	-0.64	*O*-demethylation	○	○
M3	15.31	$C_{22}H_{26}O_7$	403.17484	-0.72	*O*-demethylation	○	○
M4	16.24	$C_{22}H_{26}O_7$	403.17490	-0.57	*O*-demethylation	○	○
M5	14.15	$C_{23}H_{28}O_8$	433.18442	-2.95	hydroxylation	○	○
M6	9.19	$C_{21}H_{24}O_7$	389.15903	-1.16	di-*O*-demethylation	○	ND
M7	11.31	$C_{21}H_{24}O_7$	389.15903	-1.16	di-*O*-demethylation	○	ND
M8	14.5	$C_{22}H_{26}O_8$	419.17090	2.05	*O*-demethylation & hydroxylation	○	○
M9	5.08	$C_{28}H_{34}O_{13}$	596.23291*	-1.46	*O*-demethylation & glucuronidation	○	○
M10	5.39	$C_{28}H_{34}O_{13}$	596.23297*	-1.36	*O*-demethylation & glucuronidation	○	○
M11	6.72	$C_{28}H_{34}O_{13}$	596.23395*	0.29	*O*-demethylation & glucuronidation	○	○
M12	7.87	$C_{28}H_{34}O_{13}$	596.23303*	-1.26	*O*-demethylation & glucuronidation	○	○
M13	6.35	$C_{22}H_{26}O_{10}S$	500.15787*	-1.26	*O*-demethylation & sulfation	○	○
M14	7.79	$C_{22}H_{26}O_{10}S$	500.15793*	-1.14	*O*-demethylation & sulfation	○	○
M15	3.54	$C_{27}H_{32}O_{13}$	582.21747*	-1.13	di-*O*-demethylation & glucuronidation	○	ND
M16	3.22	$C_{21}H_{24}O_{10}S$	469.11548	-1.75	di-*O*-demethylation & sulfation	○	ND
M17	3.52	$C_{21}H_{24}O_{10}S$	469.11659	0.62	di-*O*-demethylation & sulfation	○	ND
M18	4.55	$C_{21}H_{24}O_{10}S$	469.11588	-0.89	di-*O*-demethylation & sulfation	○	ND
M19	1.22	$C_{21}H_{24}O_{13}S_2$	566.09906*	-1.08	di-*O*-demethylation & di-sulfation	○	ND

ND: not detected

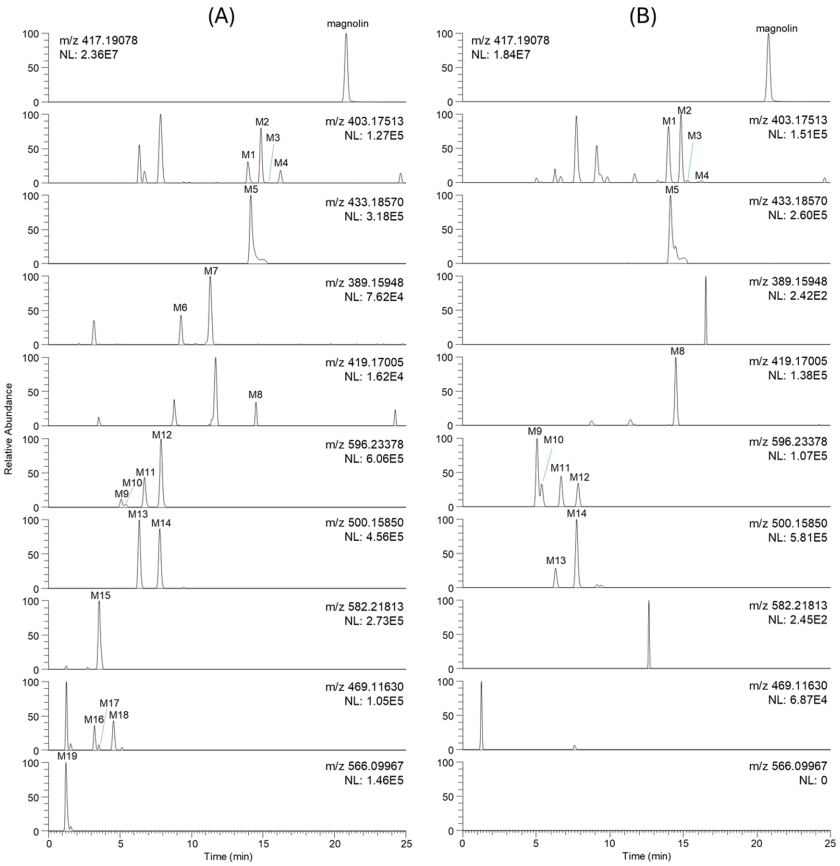

Figure 1. Extracted ion chromatograms of magnolin and its possible metabolites after incubation of 10 μM magnolin with (A) human and (B) rat hepatocytes at 37°C for 2 h.

c]furan-1-ylium ion], *m/z* 249.11217 [4-(3,4-dimethoxyphenyl)tetrahydro-1*H*,3*H*-furo[3,4-c]furan-1-ylium ion], *m/z* 219.10172 [(2,3-dihydrofuran-3-yl)(3,4-dimethoxyphenyl)methylium ion], *m/z* 189.09117 [2-(3,4-dimethoxybenzyl)cycloprop-2-en-1-ylium ion], *m/z* 181.08603 [(3,4,5-trimethoxyphenyl)methylium ion], and *m/z* 151.07545 [(3,4-dimethoxyphenyl)methylium ion] (Figure 2A).

M1 and M3 showed the $[M+H]^+$ ion at *m/z* 403.17496, which is 14 atomic mass units (amu) less than the $[M+H]^+$ ion of magnolin. The MS/MS spectra of M1 and M3 included product ions at *m/z* 385.16440 (loss of water from $[M+H]^+$ ion), *m/z* 314.11462, *m/z* 265.10663 [4-(3-hydroxy-3,5-dimethoxyphenyl)tetrahydro-1*H*,3*H*-furo[3,4-c]furan-1-ylium or 4-(3-hydroxy-4,5-dimethoxyphenyl)tetrahydro-1*H*,3*H*-furo[3,4-c]furan-1-ylium ion], *m/z* 249.11203, *m/z* 219.10149, *m/z* 189.09108, *m/z* 167.07005 [(4-hydroxy-3,5-dimethoxyphenyl)methylium or (3-hydroxy-4,5-dimethoxyphenyl)methylium ion], *m/z* 151.07530 (Figure 2B). According to the previous reports, magnolin was metabolized to 4″-*O*-desmethylmagnolin in the rats and in human liver microsomal incubation via demethylation at the 4″ position of the 3″,4″,5″-trimethoxyphenyl moiety.[11,12] The incubation of magnolin with human and rat liver microsomal incubation in the presence of NADPH resulted in the formation of M1 as the predominant metabolite compared to M3. Based on these results, M1 and M3 were characterized as *O*-desmethylmagnolin via *O*-demethylation at 4-methoxy group and 3-/5-methoxy group of 3,4,5-trimethoxyphenyl moiety, respectively.

M2 and M4 showed the $[M+H]^+$ ion at *m/z* 403.17487, which is 14 amu less than the $[M+H]^+$ ion of magnolin. The MS/MS spectrum of M2 showed the product ions at *m/z* 385.16434, *m/z* 314.11481, *m/z* 279.12238, *m/z* 235.09610 [4-(4-hydroxy-3-methoxyphenyl)tetrahydro-1*H*,3*H*-furo[3,4-c]furan-1-ylium or 4-(3-hydroxy-4-methoxyphenyl)tetrahydro-1*H*,3*H*-furo[3,4-c]furan-1-ylium ion], *m/z* 205.08583 [(2,3-dihydrofuran-3-yl)(4-hydroxy-3-methoxyphenyl)methylium or (2,3-dihydrofuran-3-yl)(3-hydroxy-4-methoxyphenyl)methylium ion], *m/z* 181.08583, *m/z* 175.07526 [2-(4-hydroxy-3-methoxybenzyl)cycloprop-2-en-1-ylium or 2-(3-hydroxy-4-methoxybenzyl)cycloprop-2-en-1-ylium ion], and *m/z* 137.05965 [(4-hydroxy-3-methoxyphenyl)methylium or (3-hydroxy-4-methoxyphenyl)methylium ion] (Figure 2C), suggesting that M2 and M4 were formed by *O*-demethylation at the 3,4-dimethoxyphenyl moiety. According to the previous reports,[11,12] M2 and M4 were tentatively identified as *O*-desmethylmagnolin via *O*-demethylation at 4-methoxy group and 3-methoxy group of 3,4-dimethoxyphenyl moiety, respectively.

M5 showed the $[M+H]^+$ ion at *m/z* 433.18442, which is 16 amu more than the $[M+H]^+$ ion of magnolin. The MS/MS spectrum of M5 showed the product ions at *m/z* 415.17548

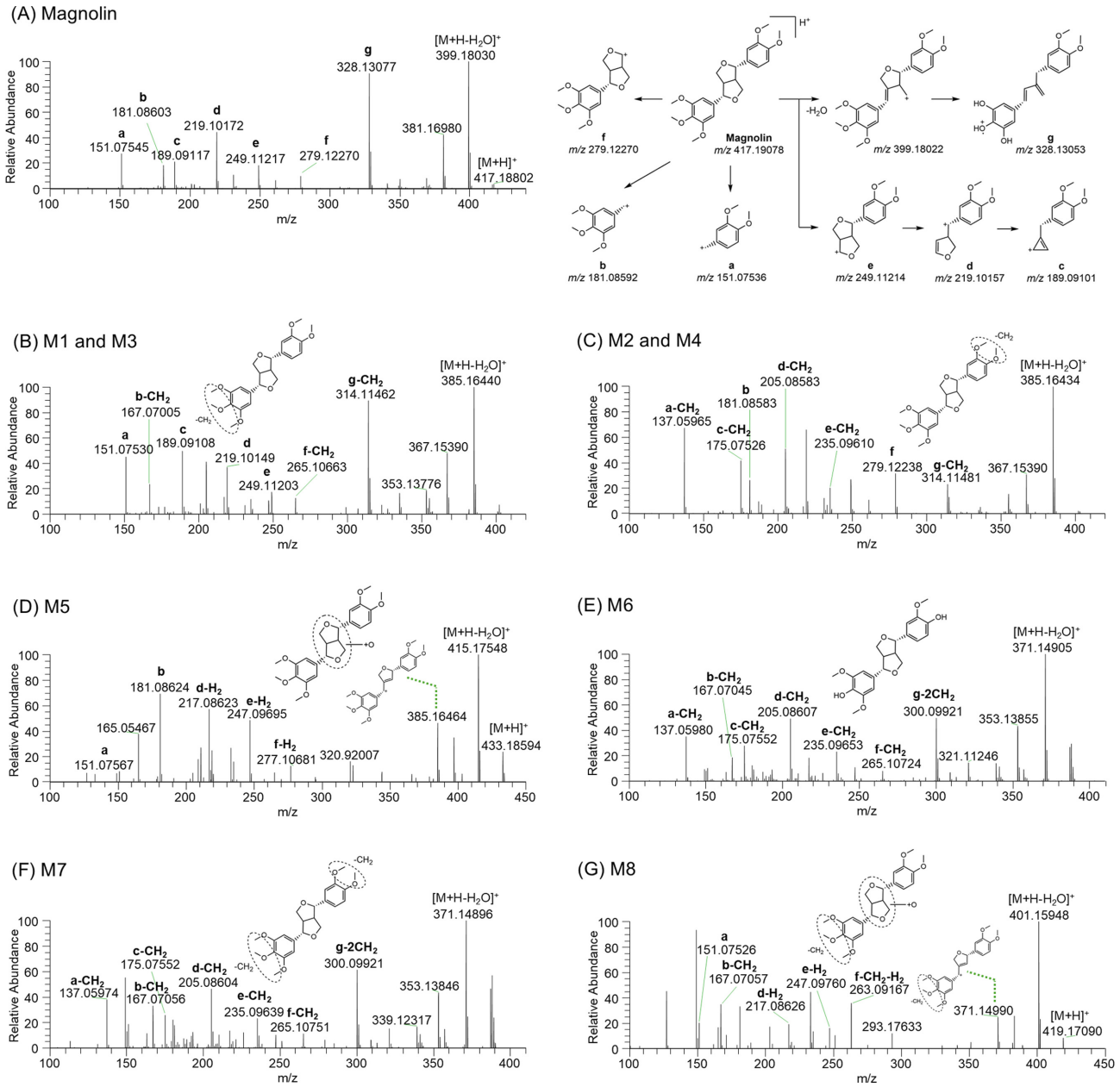

Figure 2. MS/MS spectra and fragmentation of (A) magnolin and (B–G) phase 1 metabolites. Fragments, a–g represent the characteristic product ions of magnolin.

(loss of water from $[M+H]^+$ ion), *m/z* 385.16464, *m/z* 277.10681 [4-(3,4,5-trimethoxyphenyl)-6,6a-dihydro-1*H*,3*H*-furo[3,4-c]furan-1-ylium ion], *m/z* 247.09695 [4-(3,4-dimethoxyphenyl)-6,6a-dihydro-1*H*,3*H*-furo[3,4-c]furan-1-ylium ion], *m/z* 217.08623 [(3,4-dimethoxyphenyl)(furan-3(2*H*)-ylidene)methylium ion], *m/z* 181.08624, and *m/z* 151.07567 (Figure 2D), indicating that M5 was formed by hydroxylation at tetrahydrofuran moiety, but the accurate position of hydroxylation at tetrahydrofuran moiety of M5 could not be assigned without an authentic standard.

M6 and M7 showed the $[M+H]^+$ ion at *m/z* 389.15903, which is 28 amu less than the $[M+H]^+$ ion of magnolin. The MS/MS spectra of M6 and M7 showed the product ions at *m/z* 371.14905 (loss of water from $[M+H]^+$ ion), *m/z* 300.09921, *m/z* 265.10724, *m/z* 235.09653, *m/z* 205.08607, *m/z* 175.07552, *m/z* 167.07045, and *m/z* 137.05980 (Figure 2E and 2F). M6 and M7 might be di-*O*-desmethylmagnolin formed via di-*O*-demethylation at both 3,4-dimethoxyphenyl and 3,4,5-trimethoxyphenyl moiety. M6 was confirmed as medioresinol on the basis of the retention time and MS/

MS spectrum of the authentic standard, but the accurate positions of *O*-demethylation for M7 could not be assigned without an authentic standard.

M8 showed the $[M+H]^+$ ion at *m/z* 419.17090, which is 2 amu more than the $[M+H]^+$ ion of magnolin. The MS/MS spectrum of M8 showed the product ions at *m/z* 401.15948

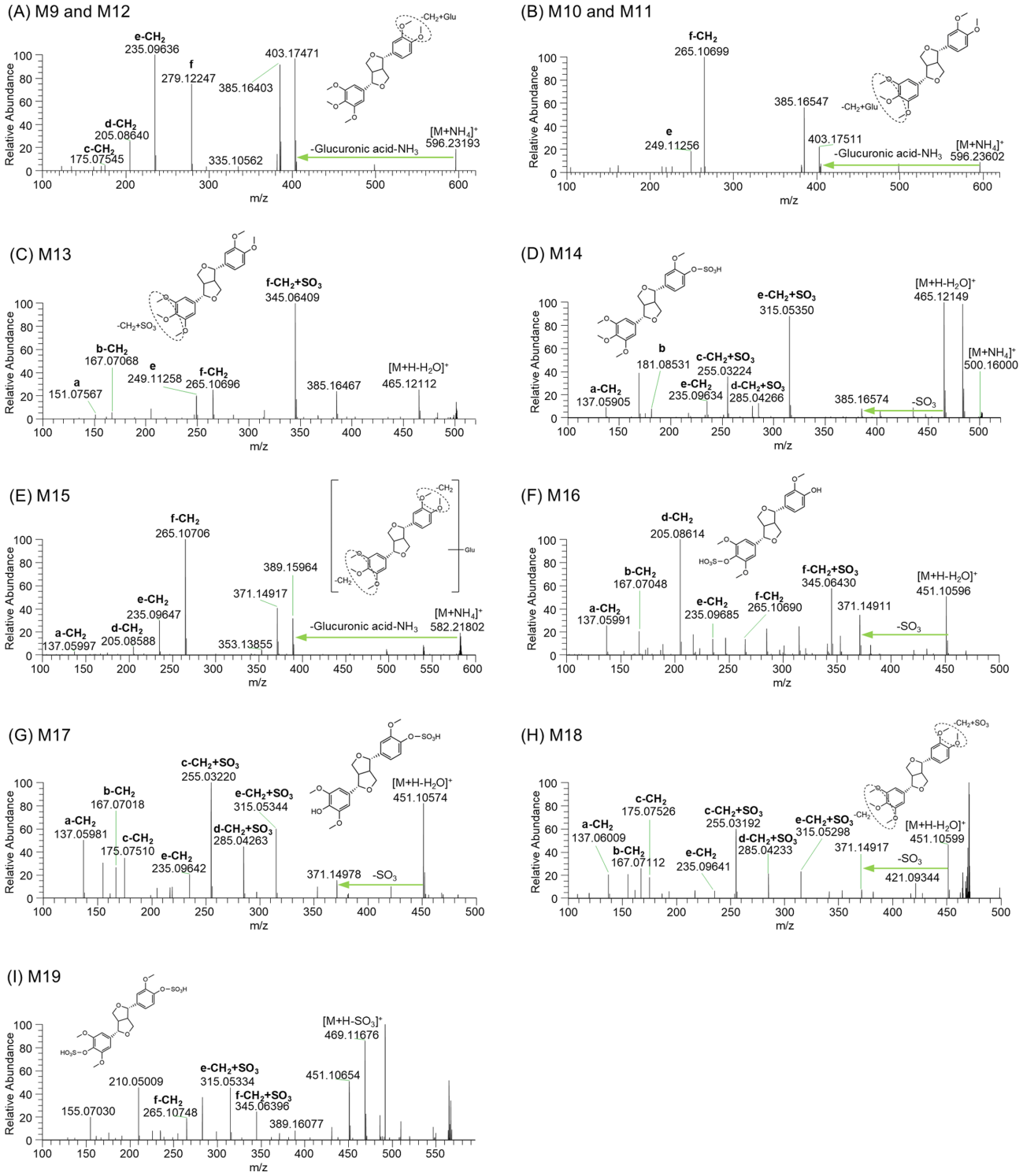

Figure 3. MS/MS spectra of phase 2 metabolites of magnolin. (A) M9 and M12, (B) M10 and M11, (C) M13, (D) M14, (E) M15, (F) M16, (G) M17, (H) M18, and (I) M19. The fragments, a–g represents the product ions of magnolin in Figure 2.

(loss of water from $[M+H]^+$ ion), *m/z* 371.14990 (loss of CH_2O from *m/z* 401.15948), *m/z* 263.09167 [1-(4-hydroxy-3,5-dimethoxyphenyl)-3a,4-dihydro-1*H*,3*H*-furo[3,4-c]furan-4-ylium or 1-(3-hydroxy-4,5-dimethoxyphenyl)-3a,4-dihydro-1*H*,3*H*-furo[3,4-c]furan-4-ylium ion], *m/z* 247.09760, *m/z* 217.08626, *m/z* 167.07057, and *m/z* 151.07526 (Figure 2G), suggesting that M8 was formed by hydroxylation at the tetrahydrofuran moiety and *O*-demethylation at 3,4,5-trimethoxyphenyl moiety, but the exact positions of these modifications could not be assigned without an authentic standard.

M9, M10, M11, and M12 showed the $[M+NH_4]^+$ ion at *m/z* 596.23291, which is 193 amu more than the $[M+H]^+$ ion of *O*-desmethylmagnolin. The MS/MS spectra of M9 and M12 showed the product ions at *m/z* 403.17471 (loss of glucuronosyl group and NH_3 from $[M+NH_4]^+$ ion), *m/z* 385.16403 (loss of water from *m/z* 403.17471), *m/z* 279.12247, *m/z* 235.09636, *m/z* 205.08640, and *m/z* 175.07545 (Figure 3A), indicating that M9 and M12 were glucuronides of M2 and M4, respectively. The MS/MS spectra of M10 and M11 showed the product ions at *m/z* 403.17511, *m/z* 385.16457, *m/z* 265.10699, and *m/z* 249.11256 (Figure 3B), indicating that M10 and M11 were glucuronides of M1 and M3, respectively. According to the previous report, 4′-*O*-desmethylmagnolin and 4′′-*O*-desmethylmagnolin were identified after treatment of rat urine samples with β-glucuronidase[11]. Rat liver microsomal incubation of magnolin in the presence of NADPH and UDPGA resulted in the formation of M9 and M10 with negligible amounts of M11 and M12. Based on these findings, M9, M10, M11, and M12 were tentatively identified as M2 glucuronide, M1 glucuronide, M3 glucuronide, and M4 glucuronide, respectively.

M13 and M14 showed the $[M+NH_4]^+$ ion at *m/z* 500.15787, which is 97 amu more than the $[M+H]^+$ ion of *O*-desmethylmagnolin, suggesting the sulfation of *O*-desmethylmagnolin. The MS/MS spectrum of M13 included *m/z* 465.12112 (loss of water and NH_3 from $[M+NH_4]^+$ ion), *m/z* 345.06409 [4-(3,5-dimethoxy-4-(sulfooxy)phenyl)tetrahydro-1*H*,3*H*-furo[3,4-c]furan-1-ylium or 4-(3,4-dimethoxy-5-(sulfooxy)phenyl)tetrahydro-1*H*,3*H*-furo[3,4-c]furan-1-ylium ion], *m/z* 265.10696, 249.11258, 167.07068, and 151.07567 (Figure 3C), indicating that M13 was formed by *O*-demethylation and sulfation at the 3,4,5-trimethoxyphenyl moiety. The MS/MS spectrum of M14 included *m/z* 465.12112, *m/z* 315.05350 [4-(3-methoxy-4-(sulfooxy)phenyl)tetrahydro-1*H*,3*H*-furo[3,4-c]furan-1-ylium ion], *m/z* 285.04266 [2,3-dihydrofuran-3-yl)(3-methoxy-4-(sulfooxy)phenyl)methylium ion], *m/z* 255.03224 [2-(3-methoxy-4-(sulfooxy)benzyl)cycloprop-2-en-1-ylium ion], 235.09634, 181.08531, and 137.05905 (Figure 3D), suggesting that M14 was formed by *O*-demethylation and sulfation at the 3′,4′-dimethoxy moiety. Sulfatase treatment of human liver S9 fraction incubates of magnolin in the presence of NADPH and PAPS resulted in the decrease of M14 peak and increase of M2 peak, indicating that M14 may be M2 sulfate.

M15 showed the $[M+NH_4]^+$ ion at *m/z* 582.21747, which is 193 amu more than the $[M+H]^+$ ion of di-*O*-desmethylmagnolin, suggesting the glucuronidation of di-*O*-desmethylmagnolin. The MS/MS spectrum of M15 showed the product ions at *m/z* 389.15964 (loss of glucuronosyl group and NH_3 from $[M+NH_4]^+$ ion), *m/z* 371.14917 (loss of water from *m/z* 389.15964), *m/z* 265.10706, *m/z* 235.09647, *m/z* 205.08588, and *m/z* 137.05997 (Figure 3E). Glucuronidase treatment of magnolin-treated human hepatocytes resulted in the increase of M7 peak area and the decrease of M15 peak area, indicating that M15 might be M7 glucuronide, but the accurate position of glucuronidation of M15 could not be assigned without an authentic standard.

M16, M17, and M18 showed the $[M+H]^+$ ion at *m/z* 469.11548, which is 80 amu more than the $[M+H]^+$ ion of di-*O*-desmethylmagnolin, suggesting the sulfation of di-*O*-desmethylmagnolin. The MS/MS spectrum of M16 showed *m/z* 451.10596 (loss of water from $[M+H]^+$ ion), *m/z* 371.14911 (loss of sulfate group from *m/z* 451.10596), *m/z* 345.06430, *m/z* 265.10690, 235.09685, 205.08614, 167.07048, and 137.05991, indicating the sulfation at 4-hydroxy-3,5-dimethoxyphenyl moiety (Figure 3F). The fragment ions of M17 and M18 in MS/MS spectra included *m/z* 451.10574, *m/z* 371.14978, *m/z* 315.05344, *m/z* 285.04263, *m/z* 255.03220, and *m/z* 175.07510 (Figure 3G and 3H), suggesting that M17 and M18 were formed by *O*-demethylation and sulfation at dimethoxyphenyl moiety. The incubation of medioresinol with human liver S9 fraction in the presence of PAPS resulted in the formation of two medioresinol sulfates (M16 and M17). Therefore, M16 and M17 were characterized as medioresinol (M6) sulfate via sulfation at 2,6-dimethoxyphenol moiety and 4-hydroxy-3-methoxyphenyl moiety, respectively (Figure 3F and 3G). Sulfatase treatment of magnolin treated human hepatocytes resulted in the increase in M6 and M7 peak areas and the decrease in M16, M17, and M18 peaks, indicating that M18 might be M7 sulfate.

M19 showed the $[M+NH_4]^+$ ion at *m/z* 566.09906, which is 177 amu more than the $[M+H]^+$ ion of di-*O*-desmethylmagnolin, suggesting the di-sulfation of di-*O*-desmethylmagnolin. The MS/MS spectrum of M19 showed *m/z* 469.11676 (loss of sulfate and NH_3 from $[M+NH_4]^+$ ion), *m/z* 451.10654 (loss of water from *m/z* 469.11676), *m/z* 345.06396, *m/z* 315.05334, and *m/z* 265.10748 (Figure 3I). M19 was identified as M6 (medioresinol) disulfate on the basis of its retention time and MS/MS spectrum of medioresinol disulfate obtained after incubation of mediorescinol with human liver S9 fraction in the presence of PAPS.

The incubation of magnolin with human hepatocytes resulted in the formation of eight phase 1 metabolites (M1-M8) and eleven phase 2 metabolites via glucuronidation and sulfation of phase 1 metabolites, but magnolin was

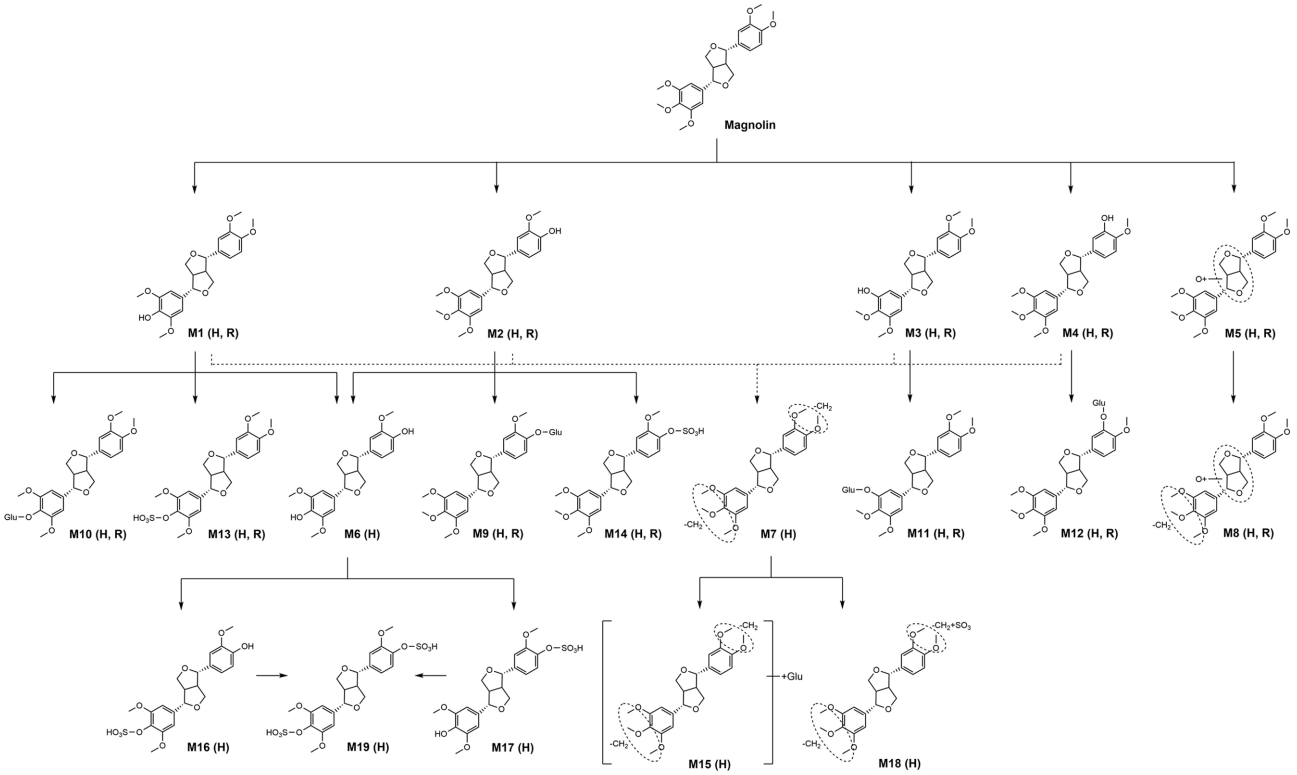

Figure 4. Possible in vitro metabolic pathways of magnolin in human (H) and rat (R) hepatocytes.

metabolized to 6 phase 1 metabolites (M1-M5, and M8) and 6 phase 2 metabolites (M9-M14) in rat hepatocytes (Figure 1, Table 2). The potential *in vitro* metabolic pathways of magnolin in human and rat hepatocytes are summarized in Figure 4.

In conclusion, the incubation of magnolin with human and rat hepatocytes produced 19 (M1-M19) and 12 (M1-M5 and M8-M14) metabolites, respectively. These included 8 phase 1 metabolites, i.e., *O*-desmethylmagnolin (M1-M4), hydroxymagnolin (M5), di-*O*-desmethylmagnolin [M6 (mediorescinol) and M7], and *O*-desmethyl-hydroxymagnolin (M8) and 11 phase 2 metabolites including M1 glucuronide (M10), M2 glucuronide (M9), M3 glucuronide (M11), M4 glucuronide (M12), M7 glucuronide (M15), M1 sulfate (M13), M2 sulfate (M14), M6 sulfates (M16 and M17), M7 sulfate (M18), and M6 disulfate (M19).

Acknowledgements

This work was supported by a grant from the National Research Foundation of Korea (NRF) funded by the Korea government (MSIT) (NRF-2023R1A2C2007632) and the Research Fund, 2024 of the Catholic University of Korea.

Conflict of interest

The authors have no conflicts of interest to declare.

References

1. Pan, J.X.; Hensens, D.H.; Zink, D.L.; Chang, M.N.; Hwang, S. *Phytochemistry* **1987**, 26, 1377. https://doi.org/10.1016/S0031-9422(00)81816-6.
2. Kim, J.Y.; Lim, H.J.; Lee da, Y.; Kim, J.S.; Kim, D.H.; Lee, H.J.; Kim, H.D.; Jeon, R.; Ryu, J.H. *Bioorg. Med. Chem. Lett.* **2009**, 19, 937. https://doi.org/10.1016/j.bmcl.2008.11.103.
3. Wang, F.; Zhang, G.; Zhou, Y.; Gui, D.; Li, J.; Xing, T.; Wang, N. *Oxid. Med. Cell. Longev.* **2014**, 2014, 203458. https://doi.org/10.1155/2014/203458.
4. Lee, C.J.; Lee, M.H.; Yoo, S.M.; Choi, K.I.; Song, J.H.; Jang, J.H.; Oh, S.R.; Ryu, H.W.; Lee, H.S.; Surh, Y.J.; Cho, Y.Y. *BMC Cancer* **2015**, 15, 576. https://doi.org/10.1186/s12885-015-1580-7.
5. Huang, Y.; Zou, X.; Zhang, X.; Wang, F.; Zhu, W.; Zhang, G.; Xiao, J.; Chen, M. *Biomed. Pharmacother.* **2017**, 87, 714. https://doi.org/10.1016/j.biopha.2017.01.010.
6. Yu, H.; Yin, S.; Zhou, S.; Shao, Y.; Sun, J.; Pang, X.; Han, L.; Zhang, Y.; Gao, X.; Jin, C.; Qiu, Y.; Wang, T. *Cell Death Dis.* **2018**, 9, 702. https://doi.org/10.1038/s41419-018-0660-4.
7. Lee, M.S.: Shim, H.J.; Cho, Y.-Y.; Lee, J.Y.; Kang, H.C.; Song, I.S.; Lee, H.S. *Arch. Pharm. Res.* **2024**, 47, 111. https://doi.org/10.1007/s12272-023-01483-w.
8. Lee, M.S.: Park, E.J.: Cho, Y.-Y.; Lee, J.Y.; Kang, H.C.; Lee, H.S. *Toxicol. Res.* **2024**, 40, 125. https://doi.org/10.1007/s43188-023-00211-2.

9. Lee, M.S.: Lee, J.; Pang, M.; Kim, J.; Cha, H.; Cheon, B.; Choi, M.-K.; Song, I.-S.; Lee, H.S. *Pharmaceutics* **2024**, 16, 799. https://doi.org/10.3390/pharmaceutics16060799.
10. Kim, N.J.; Song, W.Y.; Yoo, S.D.; Oh, S.R.; Lee, H.K.; Lee, H.S. *Arch. Pharm. Res.* **2010**, 33, 933. https://doi.org/10.1007/s12272-010-0617-3.
11. Miyazawa, M.; Kasahara, H.; Kameoka, H. *Phytochemistry* **1993**, 32, 1421. https://doi.org/10.1016/0031-9422(93)85150-P.
12. Kim, D.K.; Liu, K.H.; Jeong, J.H.; Ji, H.Y.; Oh, S.R.; Lee, H.K.; Lee, H.S. *Xenobiotica* **2011**, 41, 358. https://doi.org/10.3109/00498254.2010.549968.
13. Kim, J.H.; Kwon, S.S.; Jeong, H.U.; Lee, H.S. *Int. J. Mol. Sci.* **2017**, 18. https://doi.org/10.3390/ijms18050952.
14. Park, R.; Park, E.J.; Cho, Y.Y.; Lee, J.Y.; Kang, H.C.; Song, I.S.; Lee, H.S. *Pharmaceutics* **2021**, 13. https://doi.org/10.3390/pharmaceutics13020187.
15. Bohnert, T.; Gan, L.-S. 2009. The Role of Drug Metabolism in Drug Discovery. In *Enzyme Inhibition in Drug Discovery and Development*. 91.

